

A CHANDRA STUDY OF THE CIRCINUS GALAXY POINT-SOURCE POPULATION

F. E. BAUER,¹ W. N. BRANDT,¹ R. M. SAMBRUNA,^{1,2} G. CHARTAS,¹ G. P. GARMIRE,¹
S. KASPI,¹ AND H. NETZER³
The Astronomical Journal, in press

ABSTRACT

We have used the *Chandra X-ray Observatory* to resolve spatially and spectrally the X-ray emission from the Circinus Galaxy. We report here on the nature of the X-ray emission from the off-nuclear point sources associated with the disk of Circinus, which make up $\approx 34\%$ of the total 0.5–10 keV emission. We find that many of the serendipitous X-ray sources are concentrated along the optical disk of the galaxy, although few have optical counterparts within $1''$ of their X-ray positions down to limiting magnitudes of $m_V = 23$ – 25 . At the distance of Circinus (≈ 3.8 Mpc), their intrinsic 0.5–10 keV luminosities range from $\approx 2 \times 10^{37}$ erg s⁻¹ to $\approx 4 \times 10^{39}$ erg s⁻¹. One-fourth of the sources are variable over the duration of the 67 ks observation, and spectral fitting of these off-nuclear sources shows a diverse range of spectral properties. The overall characteristics of the point sources suggest that most are X-ray binaries and/or ultra-luminous supernova remnants within Circinus.

We are able to analyze the two strongest off-nuclear sources in greater detail and find both to have remarkable properties. The average X-ray luminosities of the two sources are 3.7×10^{39} erg s⁻¹ and 3.4×10^{39} erg s⁻¹. The former displays large and periodic flux variations every 7.5 hr and is well fit by a multicolor blackbody accretion-disk model with $T_{\text{in}} = 1.35$ keV, properties consistent with an eclipsing $\gtrsim 50 M_{\odot}$ black-hole binary. The latter appears to be a young supernova remnant, as it coincides with a non-thermal radio counterpart and an H α -detected H II region. This source exhibits both long-term (≈ 4 yr) X-ray variability and a 6.67–6.97 keV iron emission-line blend with a 1.6 keV equivalent width. These two objects further support the notion that super-Eddington X-ray sources in nearby galaxies can be explained by a mixture of intermediate-mass black holes in X-ray binaries and young supernova remnants.

Subject headings: galaxies: active — galaxies: individual (Circinus) — X-rays: galaxies — X-rays: binaries

1. INTRODUCTION

The study of X-ray emission from star-forming galaxies has long lagged behind studies in more traditional wavebands (e.g., ultraviolet, optical and radio) because of sensitivity and resolution limitations. These constraints largely restricted detailed investigations to sources in the Local Group, where only small pockets of ongoing star formation exist. The *Einstein X-ray Observatory* was the first to resolve the X-ray source populations in nearby galaxies (e.g., Helfand 1984; Fabbiano 1989), opening the study of luminous X-ray binaries (XBs) and supernova remnants (SNRs) to sources outside our own Galaxy (and the Magellanic Clouds) where there is generally less ambiguity in the distance to the source and hence its intrinsic luminosity. The brightest point sources in star-forming galaxies were found to be significantly more luminous on average than the brightest sources in the Milky Way (e.g., Fabbiano 1989). More sensitive X-ray observations of normal and star-forming galaxies with *ROSAT* and *ASCA* have shown that variable, off-nuclear point sources with super-Eddington X-ray luminosities (i.e., $L_X \gtrsim 2 \times 10^{38}$ erg s⁻¹ for $M = 1.4 M_{\odot}$) are common but generally not well understood (e.g., Colbert & Mushotzky 1999; Makishima et al. 2000; Roberts & Warwick 2000; Lira, Lawrence, & Johnson 2000).

The large improvements in spatial resolution and sensitivity recently afforded by *Chandra*, however, have begun to change

this picture. *Chandra* not only offers detailed studies of the brightest point sources in neighboring galaxies, but also studies of these sources over a broad range of galaxy types and luminosity classes, providing large samples of X-ray point sources that can be related by luminosity and spatial distribution to other properties of these galaxies such as gas mass, star formation rate and morphology (e.g., proximity to spiral arms, H II regions or globular clusters). Recent *Chandra* observations of M31 (Garcia et al. 2000), M81 (Tennant et al. 2001), M82 (Griffiths et al. 2000), NGC 3256 (P. Lira et al., in preparation), NGC 4038/39 (Fabbiano, Zezas, & Murray 2001), and NGC 4647 (Sarazin, Irwin, & Bregman 2000) are just a few of the diverse examples.

Here we perform a high-resolution X-ray study of the massive spiral known as the Circinus Galaxy (hereafter Circinus). Because of its proximity to the Galactic plane ($b = -3.8^\circ$), Circinus lay hidden until the 1970s. Freeman et al. (1977) found that Circinus lies at a distance of 3.8 ± 0.6 Mpc⁴ with an inclination of $\sim 65^\circ$ to the line-of-sight and appears to be located within a Galactic “window” with a visual absorption of $A_V = 1.5 \pm 0.2$ and a neutral hydrogen column density of $N_{\text{H}} = (3.0 \pm 0.3) \times 10^{21}$ cm⁻² [whereas neighboring regions typically have $A_V = 3.0$ and $N_{\text{H}} = (5\text{--}10) \times 10^{21}$ cm⁻²; Schlegel, Finkbeiner, & Davis 1998; Dickey & Lockman 1990].⁵ Since its discovery, numerous lines of evidence have been presented

¹ Department of Astronomy and Astrophysics, 525 Davey Lab, The Pennsylvania State University, University Park, PA 16802.

² Department of Physics & Astronomy and School of Computational Sciences, George Mason University, 4400 University Dr. M/S 3F3, Fairfax, VA 22030-4444.

³ School of Physics and Astronomy, Raymond and Beverly Sackler Faculty of Exact Sciences, Tel-Aviv University, Tel-Aviv 69978, Israel.

⁴ Assuming $H_0 = 75$ km s⁻¹ Mpc⁻¹. At this distance, $1''$ corresponds to 19 pc.

⁵ The Galactic absorption column for Circinus was calculated from A_V assuming the average ratio $N_{\text{H}}/A_V = 1.7 \times 10^{21}$ cm⁻² mag⁻¹ as determined by Diplax & Savage (1994a, b) and Lockman & Savage (1995). We caution that the actual ratio can deviate from the average by as much as a factor of two (Burstein & Heiles 1978).

indicating that this galaxy hosts a Seyfert nucleus: a prominent [O III] ionization cone (Marconi et al. 1994; Wilson et al. 2000), near-IR polarized bipolar scattering cones (Ruiz et al. 2000), a coronal line region (Oliva et al. 1994; Maiolino et al. 2000), polarized broad H α (Oliva et al. 1998; Alexander et al. 2000) and strong X-ray iron K α lines (Matt et al. 1996; Sambruna et al. 2001b). Additionally, this galaxy displays a moderate level of star formation, as indicated by H α imaging of a complex network of H II regions (e.g., $\sim 10^{7-8}$ yr old star-formation rings at ~ 40 and ~ 200 pc from the nucleus; Marconi et al. 1994; Wilson et al. 2000). Past X-ray studies have concentrated on the obscured nuclear source, with the only spatially resolved pre-*Chandra* observation of Circinus being a 4 ks *ROSAT* High-Resolution Imager (HRI) detection of the nucleus and one off-nuclear point source (Guainazzi et al. 1999).

In this paper, we study the properties of 16 X-ray point sources coincident with Circinus which have fluxes $F_{0.5-10.0 \text{ keV}} > 7 \times 10^{-15} \text{ erg cm}^{-2} \text{ s}^{-1}$. Details of the observation and reduction procedure are outlined in §2, and source identifications are discussed in §3. In §4 and §5 we discuss timing and spectroscopic analyses of the X-ray sources. We comment on the luminosity function of the point sources in Circinus in §6, and, finally, we discuss the implications of our findings in §7.

2. OBSERVATIONS AND DATA REDUCTION

Circinus was observed with the High-Energy Transmission Grating Spectrometer (HETGS; C. R. Canizares et al. in preparation) on 2000 June 6–7 with ACIS-S (G. P. Garmire et al., in preparation) in the focal plane. The HETGS provided both a zeroth-order image of Circinus on the ACIS S3 CCD and high-resolution dispersed spectra from two transmission gratings, the Medium-Energy Grating (MEG) and the High-Energy Grating (HEG), along the ACIS S0–S5 CCDs. The Circinus nucleus was placed near the aim point on the S3 chip and was observed using a subarray window of 600 rows to reduce pileup in the zeroth-order image.⁶ This particular configuration provided a frame time of 2.1 s and reduced pileup in the nucleus (i.e., the brightest X-ray source in the field) to $\approx 3\%$ and in the off-nuclear sources to $\lesssim 1\%$ (see Sambruna et al. 2001a).⁷ Events were telemetered in Faint mode, and the CCD temperature was -120°C . *Chandra* is known to experience periods of especially high background which are most pronounced on the S3 chip,⁸ but such “flares” are much less frequent when the HETGS is inserted.⁹ We found that no background “flares” occurred during this observation.

Analysis was performed on reprocessed *Chandra* data (2000 December reprocessing) primarily using the CIAO V2.0 software provided by the *Chandra* X-ray Center (CXC), but also with FTOOLS and custom software. We removed the 0.5 pixel randomization, performed standard ASCA grade selection, and excluded bad pixels and columns. The observation was split into two continuous segments separated by 1,270 s because the HETGS was not fully inserted during the first segment (~ 0.3 from full insertion). While the HETGS misalignment had a pro-

found effect on the gratings data, changes to the zeroth-order imaging and spectroscopy should be negligible.¹⁰ The total net exposure times for these two segments were 6,933 s and 60,153 s, respectively. The two datasets were merged (67,086 s) to enhance source detection and timing analysis. Since the telescope did not move between the two exposures, we also extracted spectra using the full exposure. Event PI values and photon energies were determined using the latest gain files appropriate for the observation. The X-ray spectra were analyzed using XSPEC (Arnaud 1996). Unless stated otherwise, spectral parameter errors are for 90% confidence assuming one parameter of interest.

The X-ray fluxes and absorption-corrected luminosities for all sources with more than 90 counts were calculated from spectral fitting using XSPEC. For sources below this count limit, fluxes and luminosities were estimated assuming an average power-law spectrum with photon index $\Gamma = 1.76$ and $N_{\text{H}} = 1.5 \times 10^{22} \text{ cm}^{-2}$ as determined from the best-fit values to sources above the 90 count limit. These flux and luminosity estimates are assumed throughout the paper unless stated otherwise. The scatter in the observed values of Γ and N_{H} suggests that there is likely to be some systematic uncertainty in our low-count flux and luminosity estimates. To assess this potential uncertainty, we replaced the average Γ and N_{H} values with the entire range of values for sources with more than 90 counts, rather than the average values. This led to deviations of no more than 36% above and 24% below the average flux and 54% above and 15% below the average absorption-corrected luminosity. We also note that the average value of N_{H} used above is much larger than the Galactic absorption column ($3 \times 10^{21} \text{ cm}^{-2}$) and has a large dispersion ($8 \times 10^{21} \text{ cm}^{-2}$), implying that there is likely to be a wide range in N_{H} values among individual sources.

3. SOURCE DETECTION AND DISTRIBUTION

Figure 1 shows an HETGS zeroth-order “false color” image of Circinus. The colors red, green, and blue represent the soft (0.5–2.0 keV), medium (2.0–4.0 keV), and hard (4.0–10.0 keV) X-ray emission, respectively. Prior to combination, each color image was smoothed with an adaptive kernel algorithm (Ebeling, White, & Rangarajan 2001) which permits the simultaneous viewing of compact and extended sources. The smoothed images each have a signal-to-noise ratio of 2.5 per smoothing beam and were corrected for exposure. Several features in the HETGS image are evident: (1) a central, bright point source, (2) a circumnuclear diffuse reflection component, (3) a soft X-ray plume coincident with the known ionization cone, and (4) several off-nuclear point sources.¹¹ The point-source distribution is elongated in the same direction as the projected major axis of the optical disk (a position angle of about -45° East of North), with the majority of the sources concentrated towards the nucleus. We see a prominent division of the circumnuclear reflection halo in Figure 1 into hard (blue) and soft (red) X-ray

⁶ Pileup is the coincidence of two or more photons in a pixel per ACIS frame that are counted by the instrument as a single, higher energy event. The presence of pileup results in photometric inaccuracy as well as in distortions to the HRMA+ACIS point spread function and to ACIS spectra.

⁷ The frame time is the fundamental unit of exposure for readout of the ACIS CCDs. The default frame time is 3.2 s, but it can range from 0.2–10.0 s, depending on the number of ACIS chips and subarray used.

⁸ See http://asc.harvard.edu/cal/Links/Acis/acis/Cal_prods/bkgnd/10_20/bg201000.html.

⁹ See <http://space.mit.edu/HETG/flight/status.html>.

¹⁰ See http://space.mit.edu/HETG/technotes/offset_effect_000619.txt.

¹¹ We note that there may be another diffuse emission component arising from unresolved point sources and/or ionized gas associated with the optical star-forming disk. However, this X-ray emission is diluted by the bright reflection halo that extends out to large radii ($> 1'$ from the nucleus).

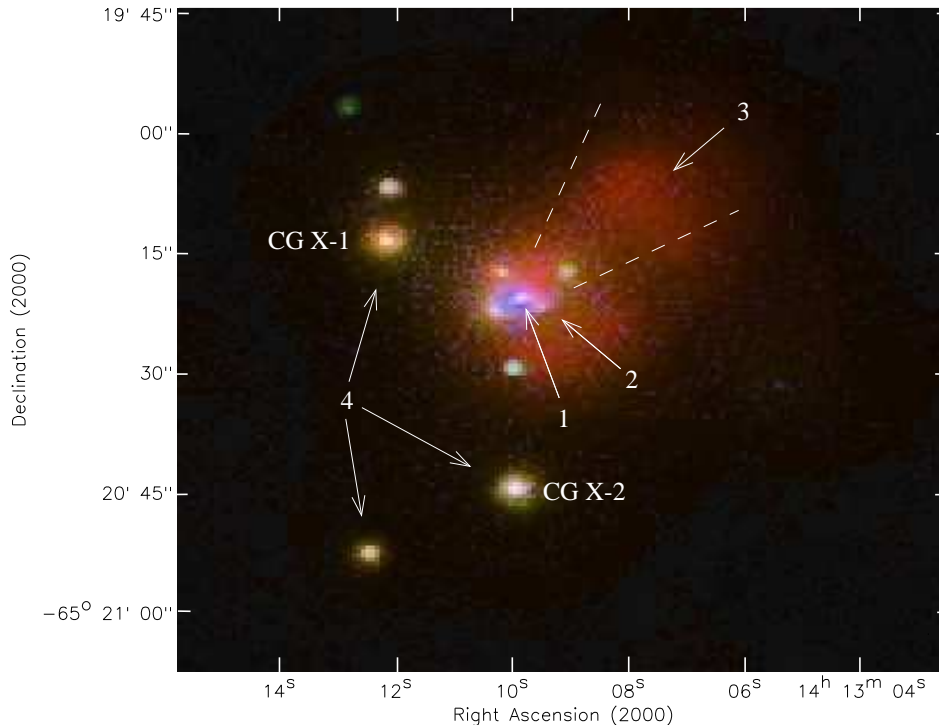


FIG. 1.— An HETGS zeroth-order “false color” $80'' \times 80''$ image of Circinus with red, green, and blue representing 0.5–2.0 keV, 2.0–4.0 keV, and 4.0–10.0 keV emission, respectively. Prior to combination, each color image was smoothed with an adaptive kernel algorithm (Ebeling, White, & Rangarajan 2001) to enhance diffuse features. The emission features depicted are (1) a central point source, (2) a diffuse circumnuclear reflection halo, (3) a soft X-ray plume coincident with the known ionization cone, and (4) several off-nuclear point sources. Most of the off-nuclear sources appear to lie along the projected major axis of the galaxy with a position angle of about -45° East of North). The dashed lines represent the opening angle of the [O III] and $H\alpha$ detected ionization cone (Marconi et al. 1994; Wilson et al. 2000). The two brightest off-nuclear X-ray sources, CG X-1 and CG X-2, are marked.

emission which appears to be perpendicular to the optical disk of the galaxy. This division is indicative of intrinsic absorption and implies that there is a large gas and dust reservoir lying in the plane of the galaxy near the nucleus. This is consistent with the large absorption suggested from infrared observations of the nuclear region (Ruiz et al. 2000).

The first three features of Circinus are discussed in Sambruna et al. (2001a, b). In the following analysis, we focus on the zeroth-order imaging and moderate-resolution spectroscopy of the fourth component. We used the CIAO source detection tool `wavdetect` (Freeman et al. 2001) to identify all point sources above a threshold significance of 10^{-7} . A total of 16 sources were found. Table 1 lists these sources along with their 0.5–10 keV fluxes, luminosities and spectral characteristics (see §5). Point-source counts and spectra were extracted using the 95% encircled-energy radii at 1.5 keV (4 pixels on-axis and up to 7–8 pixels $2'$ off-axis)¹² for all sources except CXOU J141309.2–652017, CXOU J141310.0–652021, CXOU J141310.3–652017, and CXOU J141310.4–652022. For these sources, the 90% encircled-energy radii were used to limit the amount of contamination from the diffuse circumnuclear emission component (for details on this diffuse component, see Sambruna et al. 2001a). The background-subtracted counts measured from the 90% and 95% encircled-energy radii were multiplied by 1.11 and 1.05 to obtain the aperture-

corrected count values given in column 2 of Table 1. Since some sources are embedded in diffuse emission well in excess of the typical 0.07 cts pixel $^{-1}$ background for this observation, we extracted background counts using circular or annular regions of 100–1000 pixels adjacent to or surrounding the source extraction region. Our absorbed, background-subtracted point-source detection limit is 7 counts, corresponding to an absorbed flux of $F_{0.5-10 \text{ keV}} = 7 \times 10^{-15}$ erg cm $^{-2}$ s $^{-1}$ or an absorption-corrected luminosity of $L_{0.5-10 \text{ keV}} = 2 \times 10^{37}$ erg s $^{-1}$ (assuming an average power-law spectrum with photon index $\Gamma = 1.76$ and $N_H = 1.5 \times 10^{22}$ cm $^{-2}$).

The optical nature of these serendipitous X-ray sources was assessed using *HST* WFPC2 (F502N, F547M, F606W, F656N and F814W) archival images; see Table 2 for details. The images were processed through the Space Telescope Science Institute pipeline.¹³ When multiple images in a given filter were available, the images were combined to reject cosmic rays using the IRAF task `crrej`. The automatic star-finding algorithm `daofind` in DAOPHOT (Stetson 1987) was used to generate a preliminary list of stars detected in each chip for each filter. We then performed aperture photometry to determine each star’s instrumental magnitude using 2-pixel radius apertures in the WF chips and 5-pixel radius apertures in the PC chip. Aperture corrections to a $0''.5$ radius were then determined from bright stars on each chip.

¹² E. D. Feigelson 2001, private communication; see also http://asc.harvard.edu/cal/Links/Acis/acis/Cal_prods/psf/analysis.html

¹³ See <http://www.stsci.edu/documents/dhb/web/DHB.html>.

TABLE 1
X-RAY SOURCES IN THE ACIS-S3 IMAGE OF CIRCINUS

(1) CXOU J Source	(2) Counts	(3) P_{con}	(4) m_V	(5) F_X	(6) L_X	(7) $\log(F_X/F_V)$	(8) N_{H}	(9) Γ	(10) Comments
141257.8–651425	38.0 ± 10.9	97.3	> 20.7 (DSS)	0.040^\dagger	0.116^\dagger	> 0.25	
141303.3–652043	17.4 ± 6.5	42.6	22.1 (<i>HST</i>)	0.019^\dagger	0.053^\dagger	0.49	
141305.5–652031	21.3 ± 7.0	38.6	> 25.3 (<i>HST</i>)	0.023^\dagger	0.065^\dagger	> 1.85	
141307.5–652106	7.7 ± 3.9	8.4	22.2 (<i>HST</i>)	0.007^\dagger	0.020^\dagger	0.10	Variable (flare)
141309.2–652017	99.1 ± 12.0	43.8	> 23.4 (<i>HST</i>)	0.10	0.24	> 1.73	0.99 (< 4.87)	$1.44^{+1.36}_{-0.93}$	
141309.7–652211	11.9 ± 4.6	29.8	> 20.7 (DSS)	0.011^\dagger	0.032^\dagger	> -0.31	
141310.0–652021	6571.2 ± 81.4	85.6	~ 19.0 (<i>HST</i>)	12.3	23.3	Nucleus
141310.0–652044 (CG X-2)	1374.5 ± 37.1	76.0	22.2 (<i>HST</i>)	1.33	3.43	2.61	$1.14^{+0.29}_{-0.26}$	$1.77^{+0.21}_{-0.22}$	Long-term variable, 6.9 keV emission line, embedded in HII region (<i>HST</i>)
141310.1–651832	15.9 ± 5.7	54.5	> 20.9 (DSS)	0.017^\dagger	0.048^\dagger	> -0.04	
141310.1–652029	166.0 ± 15.0	93.2	> 25.3 (<i>HST</i>)	0.17	0.73	> 2.28	$3.37^{+3.49}_{-2.95}$	$2.03^{+1.14}_{-0.92}$	
141310.3–652017	342.5 ± 20.6	85.1	> 25.3 (<i>HST</i>)	0.26	1.40	> 1.94	$1.26^{+0.68}_{-0.65}$	$2.72^{+0.51}_{-0.52}$	
141310.4–652022	792.7 ± 29.7	2.3	> 25.3 (<i>HST</i>)	1.08	2.09	> 3.08	$0.91^{+0.65}_{-0.43}$	$0.68^{+0.31}_{-0.20}$	Variable (rise)
141312.2–652007	186.0 ± 14.9	0.9	20.1 (DSS)	0.21	0.52	0.73	1.64 (< 4.22)	$1.37^{+0.80}_{-0.84}$	Variable (flare)
141312.3–652013 (CG X-1)	1095.2 ± 34.2	0.0	> 25.3 (<i>HST</i>)	0.90	3.71	> 3.44	$1.26^{+0.28}_{-0.22}$	$2.40^{+0.22}_{-0.19}$	Variable (periodic)
141312.6–652052	119.2 ± 12.2	0.4	> 25.3 (<i>HST</i>)	0.12	0.33	> 1.65	1.43 (< 5.26)	$1.63^{+1.61}_{-0.64}$	Variable (flare)
141312.9–651957	27.7 ± 7.1	16.8	> 18.1 (DSS)	0.029^\dagger	0.084^\dagger	> -0.93	
1' radius aperture	11760 ± 152	4.2		10.0	17.2				

Note. — Column 1: Source name given as CXOU JHHMMSS.S+DDMMSS. The final row lists the global properties of Circinus determined within a 1' aperture radius of the nucleus using software provided by A. Vikhlinin (http://asc.harvard.edu/cgi-gen/contributed_software.cgi). Column 2: Background-subtracted, aperture-corrected 0.5–10.0 keV counts accumulated over 67 ks. Aperture photometry was performed using 90% and 95% encircled-energy radii for 1.5 keV, and individual background regions were selected adjacent to each source as noted in §3. The standard deviation for the source and background counts are computed following the method of Gehrels (1986) and are then combined following the “numerical method” described in §1.7.3 of Lyons (1991). Column 3: The probability that the source count rate is consistent with a constant rate, as derived from the Kolmogorov-Smirnov test (in percent). Column 4: Visual magnitudes or lower limits as determined from *HST* or DSS images (see §3). Column 5: Observed 0.5–10.0 keV fluxes in units of 10^{-12} erg cm^{-2} s^{-1} from the best-fit models to the ACIS spectra. Fluxes for sources denoted by a † were calculated assuming an average power-law spectrum with $N_{\text{H}} = 1.5 \times 10^{22}$ cm^{-2} and photon index $\Gamma = 1.76$ as determined from the best-fit values of sources with more than 90 counts. Column 6: Absorption-corrected 0.5–10.0 keV luminosities in units of 10^{39} erg s^{-1} from the best-fit models to the ACIS spectra. Luminosities for sources denoted by a † were calculated with the same assumptions as outlined in Column 5. Column 7: Ratio of the 0.5–10.0 keV X-ray flux to the *V* magnitude optical flux. Column 8: Neutral hydrogen absorption column density in units of 10^{22} cm^{-2} as determined from the best-fit models to the ACIS spectra. Also listed are the 90% confidence errors calculated for one parameter of interest ($\Delta\chi^2 = 2.7$). Column 9: Power-law photon index Γ as determined from the best-fit models to the ACIS spectra. Also listed are the 90% confidence errors calculated for one parameter of interest ($\Delta\chi^2 = 2.7$). Column 10: Comments on X-ray variability and optical identifications.

TABLE 2
HST ARCHIVAL IMAGES OF CIRCINUS

(1) Filter [†]	(2) Exp. Time (s)	(3) m_{lim}	(4) Obs. Date
WFPC2 F502N	900, 900	23.3	1999 Apr. 10
WFPC2 F547M	60	23.0	1999 Apr. 10
WFPC2 F606W	200, 400	25.3	1996 Aug. 11
WFPC2 F656N	800, 800	22.7	1999 Apr. 10
WFPC2 F814W	40	22.8	1999 Apr. 10

[†] The WFPC2 filter name denotes the central filter wavelength in nanometers and the filter width (N=narrow, M=medium, W=wide).

We aligned the *HST* images to the *Hipparcos*/*Tycho* astrometric reference frame using three moderately bright stars from the *Tycho* catalog (Høg et al. 2000) to provide absolute astrometry to $\approx 0''.4$. The F606W image had approximately the same aim point as the other WFPC2 images, but it was rotated by 130° such that most (but not all) of a $2'$ field centered on Circinus was imaged by WFPC2. We filled the slight optical coverage gap using $0''.7$ resolution 5100 \AA and 7000 \AA continuum images taken with the Superb-Seeing Imager on the New Technology Telescope (NTT) in 1994 (Figures 1 and 2 of Marconi et al. 1994). The *Chandra* zeroth-order field-of-view is significantly larger than either the *HST* or NTT images, so the optical nature of the few sources farthest from the center of Circinus was evaluated using the Digitized Sky Survey (DSS; Lasker et al. 1990). Unfortunately, the coarse resolution (FWHM $\approx 3''$) and shallow depth (limiting $m_B \approx 20$) of the DSS image in this region of the sky are not nearly as constraining as the *HST* images. The NTT and DSS images were aligned with the *HST* images using ten bright, isolated point sources in the field. The astrometric accuracy of each image is $\approx 1''.0$.

The only obvious optical counterpart to any of the X-ray sources is the nucleus of Circinus, which is offset from the X-ray nucleus centroid by $0''.7$. Given the slight uncertainty in the astrometry of the *HST* images, this value is consistent with the typical astrometric accuracy for reprocessed *Chandra* data (i.e., $\lesssim 0''.6$).¹⁴ Aligning the images based on this shift, we found that three of the off-nuclear X-ray sources are coincident with *HST* optical counterparts to within $0''.5$: an $m_V = 22.1$ counterpart with CXOU J141303.3–652043, an $m_V = 22.2$ counterpart with CXOU J141307.5–652106, and an $m_V = 22.8$ counterpart with CXOU J141310.0–652044. Johnson *V* magnitudes for these sources were calculated using SYNPHOT assuming a spectral slope determined from their $m_{F814} - m_{F547}$ color. For X-ray sources without *HST* detections, *V* magnitude limits were calculated using SYNPHOT assuming a spectral slope determined from the average $m_{F814} - m_{F547}$ color for sources in the field (i.e., $m_{F814} - m_{F547} \approx 1.4$). Several of the detected X-ray sources, however, fall outside of the range of the *HST* observations. Inspection of the NTT 5100 \AA continuum and DSS images reveals an $m_V = 20.1$ counterpart at a distance of $0''.8$ from another source (CXOU J141312.2–652007). Johnson *V*

¹⁴ See http://asc.harvard.edu/mta/ASPECT/cel_loc/cel_loc.html.

¹⁵ Johnson *B* and *R* magnitudes were derived from the United States Naval Observatory A2.0 Catalog *O* and *E* plate magnitudes using using $B = O - 0.119(O - E)$ and $R = E$ (Evans 1989).

¹⁶ The typical X-ray-to-optical flux ratios derived by Maccacaro et al. (1988) for individual source types were based on X-ray observations in the 0.3–3.5 keV band with low neutral hydrogen column densities. However, all of the Circinus off-nuclear sources exhibit spectral cutoffs below $\sim 1 \text{ keV}$ (see §5). Therefore, the flux ratios listed here have been corrected for the Galactic absorption column and visual extinction given in §1. The flux ratios have also been converted from 0.3–3.5 keV to 0.5–10.0 keV assuming the average power-law spectrum measured for sources in the Circinus field. Large spectral deviations from our adopted model could result in $\log(F_X/F_V)$ differences of up to ~ 0.5 –1.0.

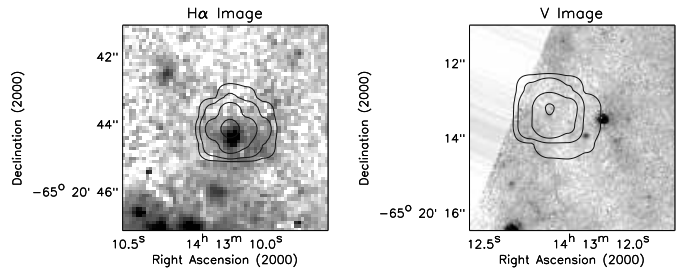


FIG. 2.— HETGS zeroth-order contours of the two brightest off-nuclear sources, CG X-2 (left) and CG X-1 (right), overlaid on *HST* F656 WF4 and F606 PC chip images, respectively. The lowest contour level is 4 counts, with each successive contour increasing by a factor of 4. CG X-2 coincides with an $m_V = 22.2$ companion embedded in a probable H II region, as indicated by the diffuse emission surrounding the optical point source in the *HST* H α image. CG X-1 has no optical counterpart to $m_V > 25.3$.

magnitudes and lower limits for sources covered by the NTT and DSS images were calculated using SYNPHOT assuming a spectral slope determined from the average $B - R$ color for sources in the field (i.e., $B - R \approx 1.25$).¹⁵

In Figure 2, we show contours of the two brightest off-nuclear X-ray sources superimposed on *HST* postage-stamp images, both of which are integral to later discussions. There is no detectable counterpart at the X-ray position of CXOU J141312.3–652013 (hereafter CG X-1). CXOU J141310.0–652044 (hereafter CG X-2) coincides with an $m_V = 22.2$ companion embedded in a probable H II region, as indicated by the diffuse emission surrounding the optical point source in the *HST* H α image in Figure 2. The bright, compact H α emission ($m_{H\alpha} = 17.9$) from this source may originate in either a compact H II region or a young SNR. In general, we found that many of the serendipitous X-ray sources appear to be coincident with optical star-forming regions: CXOU J141310.3–652017 with the inner 40 pc star-forming ring; CXOU J141310.1–652029 with the outer 200 pc star-forming ring; CG X-2 with an inter-arm H α complex; and CXOU J141309.2–652017, CXOU J141310.4–652022, CXOU J141312.2–652007 and CG X-1 with the spiral arms.

After assessing the optical properties of the X-ray point sources, we used X-ray-to-optical flux ratios to evaluate different X-ray emission mechanisms. For instance, Maccacaro et al. (1988) found that normal stars have $-4.3 < \log(F_X/F_V) < -0.3$ while background galaxies and AGN have $-1.5 < \log(F_X/F_V) < 1.9$.¹⁶ RS CVn stars, XBs and SNRs are harder to characterize because their $\log(F_X/F_V)$ ratios can range from values close to those of normal stars (RS CVn stars) up to ratios greater than 3.0 (XBs; see Maccacaro et al. 1988). This large range in X-ray-to-optical flux ratio leaves some ambiguity in the classification scheme for sources with $\log(F_X/F_V) < 1.9$, but the scheme is fairly clear cut for sources with larger ratios. In the case of Circinus, the off-nuclear sources have $\log(F_X/F_V)$ ranging from -0.9 to 3.4 (see column 7 of Table 1). We find that five off-nuclear point sources are unambiguously classified as XBs or SNRs. The remaining sources could be similarly clas-

sified, but the X-ray-to-optical flux ratios alone cannot exclude the possibility that eight sources could be background galaxies or AGN and two sources could be normal stars. We address the probability of finding foreground or background sources coincident with Circinus below.

Nearly all of the detected X-ray point sources are coincident with the disk of Circinus and lie within $2'$ of the nucleus. However, Circinus lies behind a crowded stellar region at low Galactic latitude ($b = -3.8^\circ$), so the chance superposition of Galactic X-ray sources is a valid concern. Furthermore, Circinus has a Galactic longitude of $l = 311.3^\circ$, so our line-of-sight to Circinus intersects a sizable fraction of the Galaxy. To estimate the number of foreground or background sources expected within the central region of Circinus, we used a deep *Chandra* observation of the Galactic Ridge ($l = 30^\circ$, $b = 0^\circ$; K. Ebisawa et al., in preparation). This observation is at a similar Galactic latitude and has a limiting X-ray flux of $F_{2-10 \text{ keV}} = 3 \times 10^{-15} \text{ erg cm}^{-2} \text{ s}^{-1}$. Since Circinus and the Galactic Ridge have comparable angular distances from the Galactic Center, they should also have comparable source-count distributions. In the 2–10 keV band, the Circinus zeroth-order image has a flux threshold of $F_{2-10 \text{ keV}} = 6 \times 10^{-15} \text{ erg cm}^{-2} \text{ s}^{-1}$ assuming $\Gamma = 1.76$ and $N_{\text{H}} = 1.5 \times 10^{22} \text{ cm}^{-2}$. From the Galactic Ridge measurements, we expect to detect ≈ 300 sources per deg^2 in a 67 ks *Chandra* HETGS observation, corresponding to ≈ 1.0 foreground or background sources within a $2'$ radius of Circinus at our detection threshold (see Figure 1). Therefore, most of the sources within $2'$ of the nucleus should be associated with Circinus.

Alternatively, we could ask how many sources we would expect to find in the field outside the disk of Circinus (i.e., $> 2'$ from the Circinus nucleus)? If we exclude Circinus from the ACIS S3 chip subarray, we expect to find ≈ 2 sources in the remaining area ($\approx 27 \text{ arcmin}^2$) after correcting for vignetting losses. Only one source is detected within this region (CXOU J141257.8–651425), indicating that our use of the Galactic Ridge number counts is appropriate and perhaps somewhat pessimistic.

Finally, we note that sources significantly brighter than our limiting flux have much more stringent limits. Since the *Chandra* Galactic Ridge number counts are poorly sampled above $F_{2-10 \text{ keV}} = 1 \times 10^{-13} \text{ erg cm}^{-2} \text{ s}^{-1}$, we combined them with the results of the ASCA Galactic Plane Survey (Sugizaki et al. 1999) to estimate that there is a $\lesssim 0.06\%$ chance that either of the bright off-nuclear sources shown in Figure 2 (i.e., CG X-1 and CG X-2) are foreground or background X-ray sources.

4. TIMING ANALYSIS

4.1. Short-Term Variability

The *Chandra* observation of Circinus was of sufficient duration to evaluate short-term timing characteristics for many of the off-nuclear sources. To determine objectively the existence of significant variations in the count rate, we used the Kolmogorov-Smirnov (KS) statistic to test the null hypothesis that each source plus background rate was constant over the duration of the exposure.¹⁷ Thus a source with a low KS probability (P_{con}) has a high probability of being variable ($1 - P_{\text{con}}$). Since the timing gap in the observation could lead to inaccurate variability estimates, we modified the KS test to exclude the 1.3 ks gap between the continuous 6.9 ks and 60.2 ks segments of the observation. We find that sources

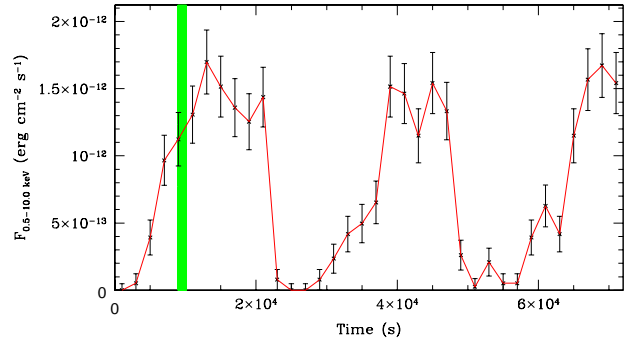


FIG. 3.— Light curve of CG X-1 over the entire duration of the observation (i.e., 6.9 ks + 1.3 ks gap + 60.2 ks) binned in 2 ks intervals. The period is 27.0 ± 0.7 ks. In that time, the flux varies by more than a factor of 20. The 1.3 ks gap (shaded band) was interpolated using the count rates found from averaging the 1 ks data segments before and after the gap. The errors bars have been calculated following the method of Gehrels (1986).

CXOU J141312.2–652007, CG X-1, and CXOU J141312.6–652052 varied at the $> 99\%$ confidence level, while sources CXOU J141307.5–652106 and CXOU J141310.4–652022 were less convincing, varying at the $\approx 92\%$ and $\approx 98\%$ confidence levels, respectively. Although CXOU J141307.5–652106 only has a KS probability of 92% and 7.7 background-subtracted counts, all of these counts were detected in a contiguous 20 ks segment of the observation, indicating it is a strong flaring source. In total, three of these short-term variable sources appeared to flare on ~ 20 ks timescales, while one exhibited a steady increase in flux over the course of the observation and another displayed periodic behavior (see below). The short-term KS statistic results for all 16 *Chandra* sources and the nature of variability observed are summarized in columns 3 and 10 of Table 1, respectively.

Many of our serendipitous X-ray sources are likely to be XBs (see §3). Since a significant fraction of XBs are X-ray pulsars with pulse periods ranging from 0.01–1,000 s (e.g., White, Nagase, & Parmar 1995), we generated power spectra for all of the Circinus X-ray sources to search for pulsations. These power spectra also allowed us to search for other periodic phenomena (e.g., eclipses or regular X-ray bursts). Only one source, CG X-1, was found to display periodic behavior above the frame-time limit of 2.1 s. Figure 3 presents the light curve of CG X-1, which shows periodic flux variability by at least a factor of 20. Because the 1.3 ks gap could introduce a small artificial dip in the light curve, we interpolated the flux values during this time using the count rates found from the 1 ks data segments before and after the gap. We used the period-fitting routine of Stetson (1996) to quantify the period and its one-sigma error as 7.5 ± 0.2 hr. To study the light curve in more detail, we folded it about its period as shown in Figure 4 to increase the signal-to-noise. The flux of the source exhibits a gradual rise early in its phase ($\sim 20\%$ of cycle), then flattens out near the peak flux ($\sim 40\%$ of cycle), and abruptly fades to a minimum near zero ($\sim 40\%$ of cycle) to close out the period. As the flux gradually increases in Figure 4 the spectrum hardens briefly, suggesting that the emission during this portion of the period may be partially absorbed at soft energies.

The simplest explanation for the variability of CG X-1 is an eclipse by an evolving binary companion, although a pure

¹⁷ The data were not binned for the KS test. The minimum time resolution was the frame time.

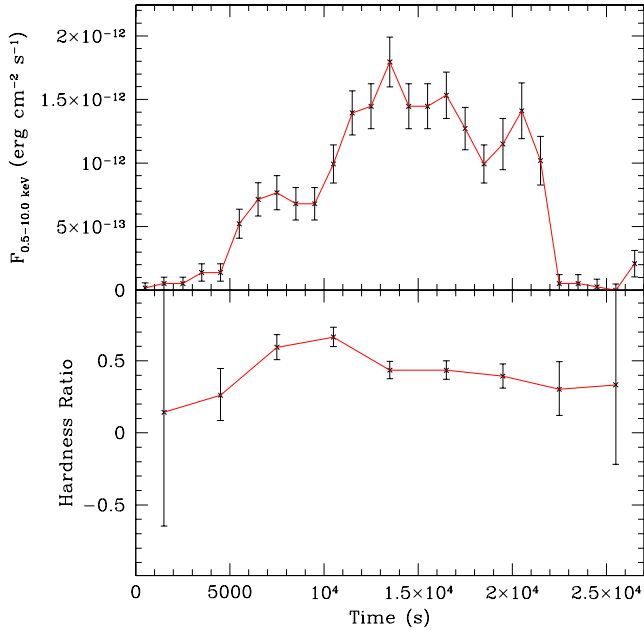


FIG. 4.— (Top) Light curve of CG X-1 folded about a period of 27.0 ks and binned in 1 ks intervals. The error bars have been calculated following the method of Gehrels (1986) assuming only photon noise. (Bottom) Hardness ratio (HR) of CG X-1 folded about a period of 27.0 ks and binned in 3 ks intervals. $HR = (H - S)/(H + S)$ where $H = 2\text{--}10$ keV counts and $S = 0.5\text{--}2$ keV counts. The errors bars for this quantity have been calculated following the “numerical method” described in §1.7.3 of Lyons (1991). Prior to folding the flux and HR light curves, the 1.3 ks gap was interpolated using the count rates found from averaging the 1 ks data segments before and after the gap.

eclipse model has difficulty explaining certain aspects of the light curve. For instance, the fraction of the period spent in eclipse is related to the size of the Roche Lobe of the binary companion and hence to the companion-to-compact-object mass ratio. We find that the eclipse fraction of CG X-1 is $\approx 40\%$, implying a mass ratio of ≈ 30 (see the Appendix of Pringle & Wade 1985). Such a large mass ratio is difficult to reconcile with other observed quantities. For instance, if CG X-1 resides in the disk of Circinus at a distance of 3.8 Mpc (see §3), then its average and peak X-ray luminosities are 3.7×10^{39} erg s $^{-1}$ and 6.6×10^{39} erg s $^{-1}$. The peak luminosity implies a compact-object mass of $M \gtrsim 50M_{\odot}$ if it is radiating at or below its Eddington luminosity. The mass limit for the compact object and the mass ratio predicted by a simple eclipse model are incompatible with the standard model of stellar evolution (i.e., a companion mass of $\gtrsim 1500M_{\odot}$ would be required). Therefore, in the context of an eclipse model, the large eclipse fraction implies that this binary system must either be experiencing strong dynamical Roche Lobe overflow, or, alternatively, the X-ray emission region must be at least partially occulted by some other means such as an accretion disk around the compact object.

Another possible scenario for generating the large-amplitude periodic variations seen from CG X-1 is by modulation of the accretion rate (e.g., from accretion-disk instabilities). One such example is the extremely variable and luminous Galactic X-ray source, GRS 1915+105. In its active state, the observed X-ray intensity of GRS 1915+105 is found to vary dramatically on timescales ranging from seconds to days, occasionally displaying quasi-periodic episodes (e.g., Greiner, Morgan, & Remillard 1996). Some of these quasi-periodic episodes coarsely re-

semble the light curve of CG X-1 (although the timescales are generally shorter for GRS 1915+105). Thus CG X-1 could also plausibly be an analog of GRS 1915+105 within Circinus.

We note that the asymmetric rise and decline in intensity of the CG X-1 light curve resembles those of AM Her type systems (e.g., Warner 1995). This class of CV typically has periods of 1–4 hr, intrinsic X-ray luminosities between $10^{31} < L_{0.5\text{--}10 \text{ keV}} < 10^{33}$ erg s $^{-1}$, and binary companions occupying a narrow range of spectral types (M2V–M6V; Cordova 1995; Verbunt & van den Heuvel 1995; Warner 1995). These characteristics restrict the X-ray-to-optical flux ratio to $3 < F_X/F_V < 300$. Given the X-ray flux associated with CG X-1 (Table 1), we would expect an M star companion to have $m_V \approx 16\text{--}20$, which is easily ruled out by the *HST* limit. The *HST* limit requires that any M2V–M6V companion star of CG X-1 be at least 1.2 kpc away. The implied X-ray luminosity ($> 10^{34}$ erg s $^{-1}$) at this distance is at least 10 times larger than the most luminous known AM Her system. Furthermore, the period (7.5 hr) is nearly two times longer than the longest period AM Her system known, and the X-ray spectrum is inconsistent with the two-component model typical of these systems (see §5). Based on these facts alone, a Galactic identification is doubtful. Moreover, the observed X-ray flux of this object limits the probability of it being a foreground source to $\lesssim 0.06\%$ (see §3). We also note that AM Her systems in particular comprise only a small fraction of all Galactic X-ray emitters ($\sim 2\%$; e.g., Motch et al. 1998). Therefore the most promising explanation for CG X-1 is an intermediate-mass black hole within Circinus.

4.2. Long-Term Variability

Circinus was also observed with the *ROSAT* HRI ($\approx 5''$ FWHM; 0.1–2.4 keV) in 1995 September (Guainazzi et al. 1999). With a total exposure time of only 4.2 ks, this HRI observation is limited to source detections above 1.7×10^{-14} erg cm $^{-2}$ s $^{-1}$ (0.5–2.0 keV). CG X-1 was detected with a 0.5–2.0 keV flux of $(8.7 \pm 2.9) \times 10^{-14}$ erg cm $^{-2}$ s $^{-1}$, a factor of ~ 2 lower than the average 0.5–2.0 keV flux measured with *Chandra* (1.7×10^{-13} erg cm $^{-2}$ s $^{-1}$), but still well within the range of intensity variations observed by *Chandra*. CG X-2, on the other hand, is completely absent from the HRI image, corresponding to a 95% confidence upper limit of 3.3×10^{-14} erg cm $^{-2}$ s $^{-1}$ (using the method of Kraft, Burrows, & Nousek 1991) in the 0.5–2.0 keV band. This is a factor of at least 11 smaller than the 0.5–2.0 keV flux of $(4.1 \pm 0.1) \times 10^{-13}$ erg cm $^{-2}$ s $^{-1}$ measured with *Chandra*. CG X-2 is coincident with an H II region, and the *Chandra* radial profile is consistent with that of a point source, indicating that this source could be either a moderately young SNR or transient XB in Circinus. Observations taken with the Australian Telescope Compact Array (ATCA) in 1995 with a beam size of $\theta_{\text{Beam}} = 0''.9 \times 0''.8$ show an unresolved radio source ($S_{3 \text{ cm}} \sim 1.2$ mJy, $\alpha_{J2000} = 14^{\text{h}}13^{\text{m}}10^{\text{s}}.0$ $\delta_{J2000} = -65^{\circ}20'44''$; M. Elmouttie, private communication) coincident to within $\lesssim 0''.6$ of the X-ray source, while none of the other radio point sources coincide with X-ray sources (see Figure 8 of Elmouttie et al. 1998). Given that there are only a few significant radio point sources in the Circinus field at a wavelength of 3 cm, the probability of this pair being a random alignment is $< 0.1\%$. The combination of bright, point-like radio, optical, and X-ray emission strongly suggests that this object is a young SNR or an H II region. We can rule out radio emission from a bright H II region, however, since the observed flux at 3 cm is approximately two orders of

magnitude higher than expected.¹⁸ A young SNR classification for CG X-2 is further supported by our spectral fitting in §5.1. The detection of a moderately strong radio source in 1995 and the lack of a bright X-ray source in 1996 is curious but not implausible given that the X-ray and radio emission are likely to result from physically distinct and separate emission regions within a young SNR (e.g., Schlegel 1995). Ongoing optical monitoring programs of Circinus over the past eight years have failed to detect any bright supernovae down to $m_V \approx 15$ (R. Evans 2000, private communication; A. Williams 2000, private communication). Thus, if CG X-2 exploded after 1993, it must have been optically faint.

5. SPECTRA

5.1. Zeroth-order

The ACIS zeroth-order spectra of the off-nuclear sources were extracted for sources with more than ≈ 90 counts using either the 90% or 95% encircled-energy extraction radii as described in §3. Circinus was placed near the node 0/1 boundary on the S3 chip, so several sources including the nucleus were dithered between nodes 0 and 1. Since the variation in the energy response of the S3 chip across these nodes is large, we chose to extract the spectra and response matrices for each node separately and fit both spectra with one model in XSPEC. To assess the spectral nature of these sources, we initially fitted the spectra with absorbed power-law models.¹⁹ We found that only one off-nuclear source required more extensive spectral modeling (CG X-2). The best-fit models with 90% confidence errors ($\Delta\chi^2 = 2.7$) are listed in columns 8 and 9 of Table 1.

The range of spectral properties for these objects is quite diverse (e.g., $\Gamma \sim 0.7$ – 2.7). All of these off-nuclear sources exhibit spectral cutoffs below ~ 1 keV that are best fitted with column densities larger than the Galactic value (see §1). These large absorption values are consistent with the fact that many of the off-nuclear X-ray sources appear to reside in star-forming regions and spiral arms in Circinus (see §3). The spectra of the two brightest off-nuclear sources have adequate counts to constrain physical models of emission and are discussed in more detail below.

In Figure 5, we present the spectrum of the periodic source CG X-1. CG X-1 happened to fall near the boundary of node 0 and node 1, such that $\approx 70\%$ of the photons from this source were dithered onto node 0 and $\approx 30\%$ onto node 1. We show the node 0 spectrum in Figure 5. This spectrum was initially fitted with a moderately soft power law with $\Gamma = 2.40^{+0.22}_{-0.19}$ and $N_H = (1.26^{+0.28}_{-0.22}) \times 10^{22} \text{ cm}^{-2}$ ($\chi^2 = 75.4$ for 59 degrees of freedom). Although this model proved acceptable, Makishima et al. (2000) have shown that the X-ray spectra of super-Eddington sources in spiral galaxies are often successfully described by multicolor disk blackbody emission (MCD; Mitsuda et al. 1984) arising from optically thick standard accretion disks around black holes. We found that a MCD model with an inner-disk temperature of $T_{in} = 1.35^{+0.13}_{-0.11}$ keV and $N_H = (6.39^{+1.57}_{-1.33}) \times 10^{21} \text{ cm}^{-2}$ worked somewhat better than the power-law model ($\chi^2 = 61.0$ for 59 degrees of freedom) and that the derived spectral parameters agree well with typical innermost disk temperatures derived for other super-Eddington sources (i.e., $T_{in} = 1.1$ – 1.8 keV; Makishima et al. 2000). Thus, we find that the spectral properties of this source are

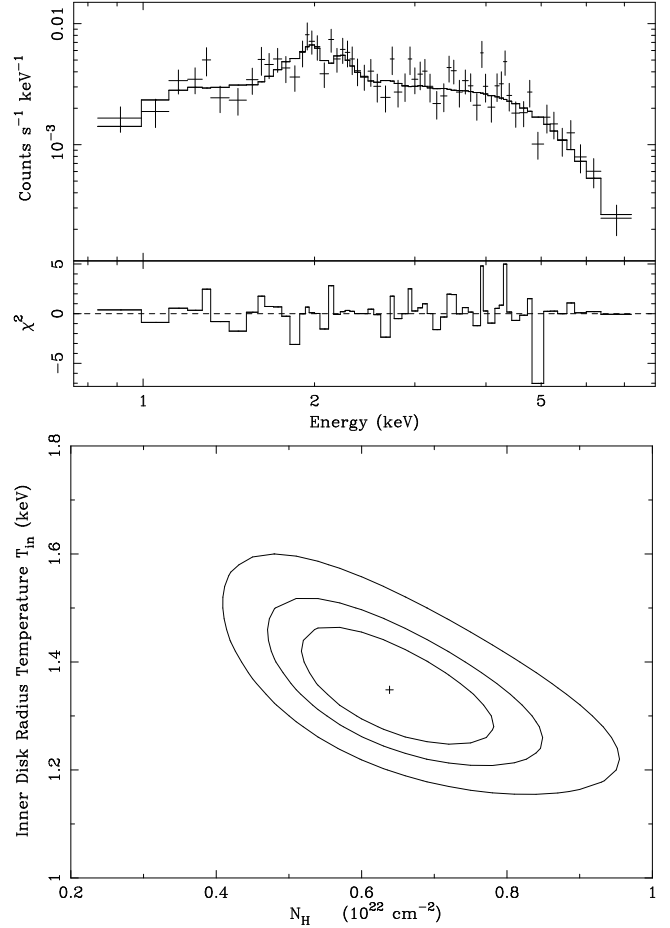


FIG. 5.— (Top) The upper panel shows the ACIS-S node 0 spectrum of CG X-1, modeled with a MCD model with an inner-disk radius temperature of $T_{in} = 1.35^{+0.13}_{-0.11}$ keV and $N_H = (6.39^{+1.57}_{-1.33}) \times 10^{21} \text{ cm}^{-2}$. The lower panel shows the residuals of the fit measured using the χ^2 statistic. (Bottom) Confidence contours between T_{in} and N_H for CG X-1. The contours represent the 68%, 90% and 99% confidence levels for two parameters of interest.

fully consistent with X-ray emission from an intermediate-mass black hole candidate in the disk of Circinus. We also attempted to fit the spectrum of CG X-1 assuming the typical spectral model for an AM Her system (i.e., the most likely Galactic candidate) to remove any remaining concerns about a possible Galactic nature of CG X-1. Spectra of AM Her systems have substantial 6.4 keV iron $K\alpha$ emission lines and continua comprised of a blackbody component with $kT_{BB} \sim 20$ eV and a bremsstrahlung component $kT_{BR} \sim 30$ keV (see §6.4 of Warner 1995). Such a model does not fit the observed spectrum well and is rejected with $\gg 99\%$ confidence.

The other bright X-ray source, CG X-2, was initially fitted with a power law with $\Gamma = 1.77^{+0.21}_{-0.22}$ and an absorption column of $N_H = (1.13^{+0.29}_{-0.26}) \times 10^{22} \text{ cm}^{-2}$ (see Figure 6). However, this fit was statistically unacceptable with $\chi^2 = 106.5$ for 74 degrees of freedom and a null-hypothesis probability of $P(\chi^2|\nu) = 8.2 \times 10^{-3}$. The spectrum shows large positive residuals around 6.9 keV. The addition of a Gaussian emission line at $6.89^{+0.04}_{-0.09}$ keV with an intrinsic line width of 190^{+57}_{-55} eV improved the fit significantly ($\chi^2 = 63.2$ for 71

¹⁸ We assume that a typical bright H II region has an electron temperature of 10^4 K, electron and proton densities of 10^2 cm^{-3} , a size of less than 10 pc (for details see Osterbrock 1989).

¹⁹ In most cases, a Raymond-Smith thermal plasma model (Raymond & Smith 1977) was equally acceptable.

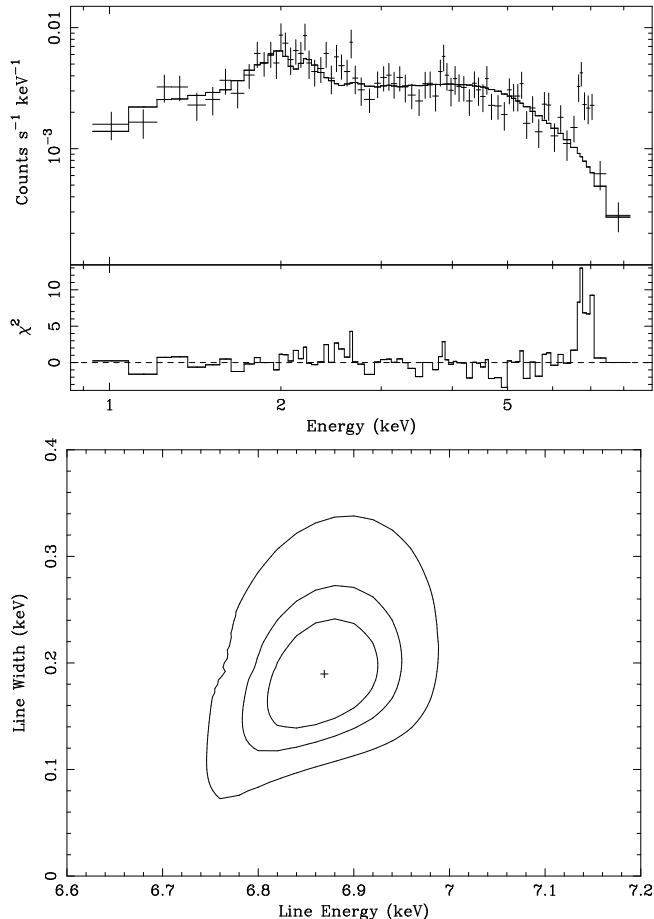


FIG. 6.— (Top) The upper panel shows the ACIS-S node 0 spectrum of CG X-2, modeled with a neutral hydrogen column of $N_{\text{H}} = (1.13^{+0.29}_{-0.26}) \times 10^{22} \text{ cm}^{-2}$ and a power law with $\Gamma = 1.77^{+0.21}_{-0.22}$. The lower panel shows the residuals of the fit measured using the χ^2 statistic. Note the large χ^2 residuals around 6.67–6.97 keV. (Bottom) The confidence contours for fit parameters of a single Gaussian emission line at 6.89 keV. The contours represent the 68%, 90% and 99% confidence levels for two parameters of interest.

degrees of freedom). The measured equivalent width of the line is $1.59^{+0.41}_{-0.46} \text{ keV}$. We note that this source is offset from the nucleus by $23''$ and totally dominates over the faint background. Furthermore, the energy of this line (6.89 keV) is quite different from the emission-line feature found in the rest of the reflection halo ($\approx 6.4 \text{ keV}$, for details see Sambruna et al. 2001a) and is not associated with that component.

To confirm that the central energy and line width of the 6.89 keV line were not due to possible calibration problems, we measured the line energies and widths of the 5.89 keV and 6.49 keV calibration lines in a calibration dataset closest to our observation date (obs62017, 2000 June 18, -120° C). From the calibration data, we extracted a large region on node 0 of the S3 chip near the position of CG X-2 and fit two Gaussian emission lines to the calibration lines using the same response matrix as used for CG X-2. The best-fit values were line energies of $5.94^{+0.01}_{-0.01} \text{ keV}$ and $6.54^{+0.01}_{-0.01} \text{ keV}$ and line widths of $53^{+03}_{-03} \text{ eV}$ and $56^{+03}_{-03} \text{ eV}$, respectively. Thus there appears to be a shift of $\approx 50 \text{ eV}$ in the central line energy and uncertainty in the line width of $\approx 60 \text{ eV}$. The true central energy of the 6.89 keV line should therefore be 6.84 keV. This 6.84 keV line is also broader than the instrumental resolution of ACIS, suggesting that it is either intrinsically broad or a blend of emission from two or

more lines.

Given the central energy of the 6.84 keV emission line, it is likely to be a blend of iron K-shell transitions at 6.67 keV (He-like line complex) and 6.97 keV (H-like line). To test this hypothesis, we modeled the spectrum of CG X-2 using two Gaussian emission components and an absorbed power law. We fixed the ratios of the He-like complex and H-like line energies and line widths to be 0.957 and 1.0, respectively, but we allowed the energy and width of the combination to vary. The normalizations of the two lines were allowed to vary independently. This model improved the χ^2 to 57.5 for 70 degrees of freedom and is better than the single Gaussian model at $\approx 99\%$ confidence using the F -test. The best-fit energies of the iron lines are $6.74^{+0.03}_{-0.03} \text{ keV}$ and $7.05^{+0.03}_{-0.03} \text{ keV}$ and are consistent with the line rest energies after removing the 50 eV blueshift due to calibration errors (see above). The intrinsic line width of each line is $70^{+38}_{-27} \text{ eV}$ and is consistent with unbroadened emission lines (compare to line widths of calibration lines above). Allowing the energies and widths of the lines to vary freely does not significantly change the best-fit results, although the errors associated with each parameter are much larger.

There are two scenarios that could explain such large equivalent width iron K-shell line emission. We first explore the possibility that this source is an X-ray binary where the strong emission lines must result from fluorescence and resonant scattering either in a wind or a corona around the accretion disk (e.g., see §1.6.2.3 of White, Nagase, & Parmar 1995). In this scenario, the direct line-of-sight to the X-ray source must be blocked; otherwise the continuum emission from the source would dilute the line emission and reduce its equivalent width below what is observed. Scattering of the continuum by electrons is relatively inefficient ($\approx 1\text{--}5\%$), so the intrinsic X-ray luminosity of this source would have to be a factor of $\approx 20\text{--}100$ times larger than observed. We also detect no short-term variability for this source, so the direct continuum would have to be blocked for more than 68 ks. Since the luminosity of this source is already $L_{0.5\text{--}10.0 \text{ keV}} = 3.4 \times 10^{39} \text{ erg s}^{-1}$ and exhibits no short-term variability, we consider an X-ray binary scenario for CG X-2 to be unlikely.

The second scenario to explain the X-ray line emission is that of a young SNR (see §4.2). Within this scenario, the line emission could be generated from either the initial forward shock that passes through the outer layers of the star and propagates into the circumstellar material or from the high-emissivity reverse shock that develops at later times. The large X-ray luminosity of CG X-2 is comparable to those of other young ($\lesssim 20 \text{ yr}$ old) SNRs detected at X-ray wavelengths (e.g., Schlegel 1995; Immler, Pietsch, & Aschenbach 1998a, b; Fox et al. 2000; Pooley et al. 2001), adding merit to such a classification. To further test this hypothesis, we fitted the spectrum with Raymond-Smith thermal plasma and non-equilibrium ionization collisional plasma models (Borkowski, Sarazin, & Blondin 1994). Figure 7 shows the best-fit model for an absorbed Raymond-Smith thermal plasma [$kT = 10.82^{+3.97}_{-2.52} \text{ keV}$, $Z = (1.35^{+0.84}_{-0.54})Z_{\odot}$, $N_{\text{H}} = (9.21^{+1.70}_{-1.48}) \times 10^{21} \text{ cm}^{-2}$]. While this model provides an acceptable fit to the data ($\chi^2 = 77.1$ for 73 degrees of freedom), it clearly underpredicts the width of the highly ionized iron emission, leaving a gap between the H-like and He-like iron lines around 6.8 keV. The non-equilibrium ionization model proved no better at fitting the broad iron-line blend.

Only ≈ 12 young SNRs have X-ray detections at all, and when adequate *ROSAT*, *ASCA* or *Chandra* spectra are

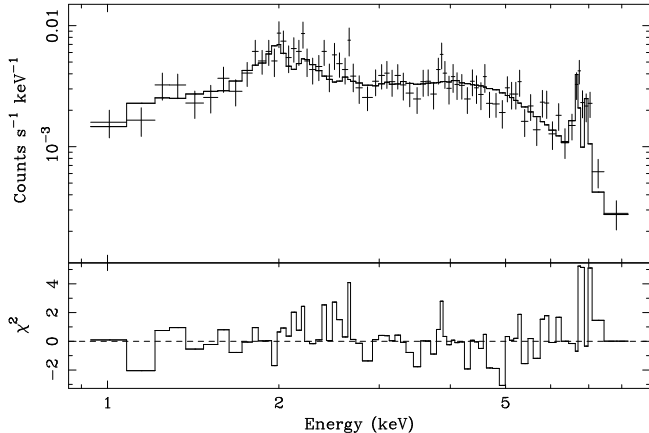


FIG. 7.— The upper panel shows the ACIS-S node 0 spectrum of CG X-2, modeled with a neutral hydrogen column of $N_{\text{H}} = (9.21^{+1.70}_{-1.48}) \times 10^{22} \text{ cm}^{-2}$, a Raymond-Smith thermal plasma model with $kT = 10.82^{+3.97}_{-2.52} \text{ keV}$ and $Z = (1.35^{+0.84}_{-0.54}) Z_{\odot}$. The lower panel shows the residuals of the fit measured using the χ^2 statistic. The emission-line blend centered at 6.89 keV is poorly fit.

available, most display high thermal temperatures ($kT = 5\text{--}10 \text{ keV}$) similar to CG X-2. Furthermore, only five young SNRs have been observed with adequate sensitivity above 5 keV to detect any K-shell iron emission. Three of these sources (SN 1986J in NGC 891, Houck et al. 1998; SN 1993J in M81, Kohmura et al. 1994; SN 1998S in NGC 3877, Pooley et al. 2001) appear to have substantial 6.8 keV iron-line emission with equivalent widths of $\approx 0.3\text{--}2 \text{ keV}$. Thus the spectrum of CG X-2 appears to be consistent with the X-ray emission seen from other young SNRs. The failure of simple physical models (e.g., a Raymond-Smith model) to fully describe the iron K-shell emission from CG X-2 is intriguing, but not implausible considering the scarcity of young, nearby SNRs and the lack of detailed X-ray spectra. In addition to highly ionized iron K-shell emission, we might expect to detect faint line emission from other highly ionized elements such as sulphur and silicon. The spectrum of CG X-2, however, is too noisy to place reliable limits on such emission.

5.2. HEG/MEG

For the two brightest off-nuclear sources, CG X-1 and CG X-2, we extracted MEG and HEG grating spectra (see Sambruna et al. 2001b for details of the extraction procedure). We found that the high-resolution spectra were consistent with the ACIS-S spectra, but that the statistics were generally poor (less than 3σ line detections in the case of CG X-2).

6. LUMINOSITY FUNCTION OF RESOLVED SOURCES

Luminosity functions (LFs) are often a useful tool for shedding physical insight into the properties of source populations. Figure 8 shows the cumulative distribution of the Circinus off-nuclear sources as a function of luminosity. For comparison, we also show three other galaxies spanning a large range of star formation rates for which similar 0.5–10.0 keV source distributions could be obtained: the Small Magellanic Cloud (SMC; Yokogawa et al. 2000), M82 (Griffiths et al. 2000) and NGC 3256 (P. Lira et al., in preparation). The LFs of these three galaxies all appear to follow the same trend such that $N \propto L_{\text{X}}^{-0.65}$. However, the LF of Circinus shows a distinct “kink” around $10^{38} - 10^{39} \text{ erg s}^{-1}$ that is not evident in the other LFs.

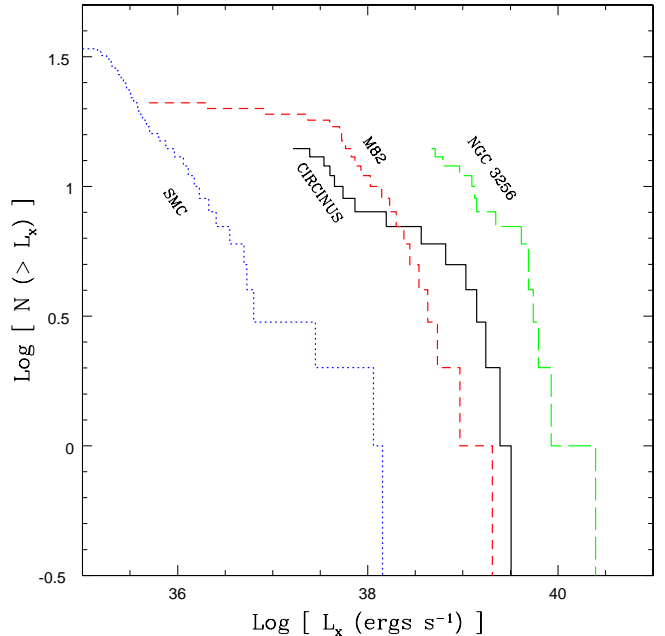


FIG. 8.— Cumulative number of sources versus 0.5–10.0 keV luminosity for Circinus (solid), the SMC (dotted), M82 (short-dashed), and NGC 3256 (long-dashed). The sources in the SMC, M82 and NGC 3256 all appear to increase with decreasing luminosity such that $N \propto L_{\text{X}}^{-0.65}$. The Circinus sources do not follow this trend (see §6).

One possible explanation for this anomalous LF may be the large attenuation of soft X-ray photons from both the large Galactic column and absorption in the HETGS. For example, if the Circinus source population has a LF slope similar to that of the other galaxies, but the low-luminosity sources in Circinus are substantially softer than the high-luminosity ones (an effect seen in NGC 4038/4039; A. Zezas et al. 2001, in preparation), a large fraction of the faint, soft X-ray sources might go undetected.

To test this hypothesis, we assumed that, in the absence of Galactic and HETGS absorption, the LF of Circinus has the same average intrinsic slope as that of the other galaxies in Figure 8 (i.e., $N \propto L_{\text{X}}^{-0.65}$). Since the brightest source detected in Circinus has a 0.5–10.0 keV luminosity of $3.4 \times 10^{39} \text{ erg s}^{-1}$, we should expect to detect ≈ 28 unabsorbed sources at the luminosity limit of our HETGS observation (i.e., $L_{0.5-10.0 \text{ keV}} = 2 \times 10^{37} \text{ erg s}^{-1}$). For simplicity, we assumed that all sources below $L_{0.5-10.0 \text{ keV}} = 1 \times 10^{38} \text{ erg s}^{-1}$ were well-fit by a power-law spectrum with an average photon index Γ . We then used PIMMS (Mukai 2000) to estimate the number of sources that would fall below our flux threshold as we varied the average Γ from 1.76 (i.e., what we find for the bright sources) to softer values, assuming an HETGS observation and an average neutral hydrogen absorption column of $N_{\text{H}} = 1.5 \times 10^{22} \text{ cm}^{-2}$. We found that in order to reproduce the observed 15 off-nuclear X-ray sources, an average photon index of $\Gamma \approx 3.2$ is necessary for the fainter sources.

While this hypothesis provides a viable explanation for the “kink” seen in the LF of Circinus, the average spectral index required for the fainter sources is significantly softer than the softest spectral index directly measured via spectral fitting analysis of the brightest sources in the field (see § 5.1 and Table 1). This large contrast argues against such a hypothesis, but we note that a similar trend of systematic softening, although con-

siderably milder, is seen in *Chandra* point-source population studies of nearby galaxies such as M81 (Tennant et al. 2001), NGC 4038/4039 (A. Zezas et al. 2001, in preparation), and NGC 4647 (Sarazin, Irwin, & Bregman 2000). The small number of counts in these studies, however, allow only crude hardness ratio determinations. Such a trend is not found in a deep *XMM-Newton* study of M31 (Shirey et al. 2001), where there are adequate counts to perform detailed spectral analysis on all sources above $L_{0.5-10.0 \text{ keV}} \approx 1 \times 10^{37} \text{ erg s}^{-1}$. Unfortunately, a large statistical sample is not yet available to clarify whether this trend of systematic spectral softening is common among the fainter point sources in nearby galaxies or whether an alternate explanation for LF of Circinus exists (e.g., there is some intrinsic difference between Circinus and the other galaxies such as morphological type, gas mass, star formation rate, star formation history, etc. which could explain the “kink”).

7. DISCUSSION AND SUMMARY

We have performed a systematic analysis of 16 point sources coincident with the disk of Circinus in a *Chandra* HETGS observation, down to a limiting X-ray luminosity of $2 \times 10^{37} \text{ erg s}^{-1}$. We find that

- Nearly half of the sources coincide with the star-forming features of the galaxy, and only four off-nuclear sources have optical counterparts.
- Four sources exhibit short-term (~ 1 day) variability, and one source exhibits only long-term (~ 4 yr) variability.
- The X-ray spectra of these objects are best-fit by a large absorption column above the Galactic value and a range of power-law photon indices from $\Gamma = 0.7-2.7$.

Based on the large observed absorption columns, spatial coincidence with the Circinus galaxy, and large X-ray-to-optical flux ratios, we conclude that the bulk of these off-nuclear sources are XBs and/or luminous SNRs located within Circinus. The shape of the Circinus LF appears to be different from those of other galaxies and may indicate a bias against faint soft X-ray sources introduced by the large Galactic column and absorption in the HETGS. Any definite conclusions about the Circinus LF, however, should wait until a large, complete sample of nearby galaxies can be assembled for comparison.

The two most luminous off-nuclear sources, CG X-1 and CG X-2, are remarkable. The distinct periodic variability, high X-ray luminosity, and soft X-ray spectrum of CG X-1 provide strong support for an interpretation as a $> 50 M_{\odot}$ black hole in an accreting binary system in Circinus. High-luminosity X-ray sources such as this one are fairly common among nearby

galaxies (see §1), but the physical nature of these objects is often poorly determined because of the limited photon statistics. The X-ray properties of the periodic source CG X-1 provide the strongest evidence to date that at least some of the super-Eddington X-ray sources detected in other galaxies are individual XBs with large inferred black-hole masses, challenging both stellar evolution and accretion disk models (e.g., Taniguchi et al. 2000; Watarai, Mizuno, & Mineshige 2001). Unfortunately, the lack of an optically detectable stellar companion limits the degree to which we can constrain the physical parameters of this system. Further X-ray observations of CG X-1 are important to tighten constraints on the variability of its period, luminosity and spectrum. If this source indeed undergoes periodic eclipses, then the period and shape of the light curve should remain fairly stable. However, if the apparent periodicity is due to accretion disk instabilities, one might expect the X-ray light curve to “evolve” away from what we see in Figure 3.

Likewise, the large X-ray luminosity, the presence of a very large equivalent width iron K-shell emission line, the hard X-ray spectrum, and the association with both a radio point source and an H α -detected H II region make CG X-2 a prime candidate for a young SNR in Circinus. Continued X-ray monitoring of this source will determine how its luminosity and spectral properties evolve with time. Nearby, X-ray-bright supernovae like CG X-2 are relatively rare (Schlegel 1995; Houck et al. 1998), but they represent an excellent opportunity to study the physical interaction of a supernova with a dense circumstellar environment.

The ubiquity of super-Eddington off-nuclear X-ray sources in nearby galaxies has become an established but poorly understood phenomenon. Our findings for Circinus support the hypothesis that the off-nuclear, super-Eddington X-ray sources in nearby galaxies are the product of *both* young SNRs and intermediate-mass black holes in XBs.

We are grateful to D. Alexander, M. Eracleous, S. Gallagher, and R. Wade for helpful discussions. We thank M. Elmouttie for information regarding radio point sources in Circinus, R. Evans and A. Williams for information on the supernova monitoring of Circinus, Y. Maeda for providing deep Galactic Ridge source counts prior to publication, A. Marconi and E. Oliva for kindly sharing their optical images of Circinus, B. McLean and J. Garcia for photographic emulsion transmission curves, and B. Wilkes for assistance with CXC data reprocessing. Support for this work was provided by the National Aeronautics and Space Administration through NASA grant NAS8-38252 (GPG, PI), NASA LTSA grant NAG5-8107 (FEB, WNB, SK) and *Chandra* Grant GO0-1160X (FEB, WNB).

REFERENCES

- Alexander, D. M., Heisler, C. A., Young, S., Lumsden, S. L., Hough, J. H., & Bailey, J. A. 2000, MNRAS, 313, 815
 Arnaud, K. A. 1996, in ASP Conf. Ser. 101, *Astronomical Data Analysis Software and Systems V*, ed. G. Jacoby, & J. Barnes (San Francisco: ASP), 17
 Begelman, M. C. 2001, ApJ, in press
 Borkowski, K. J., Sarazin, C. L., & Blondin, J. M. 1994, ApJ, 429, 710
 Burstein, D. & Heiles, C. 1978, ApJ, 225, 40
 Colbert, E. J. M., & Mushotzky, R. F. 1999, ApJ, 519, 89
 Cordova, F. 1995, in *X-ray Binaries*, ed. W. H. Lewin, J. Van Paradijs, & E. P. J. van den Heuvel (Cambridge: Cambridge University Press), p. 331
 Dickey, J. M., & Lockman, F. J. 1990, ARA&A, 28, 215
 Diplax, A. & Savage, B. D. 1994a, ApJS, 93, 211
 Diplax, A. & Savage, B. D. 1994b, ApJ, 427, 274
 Ebeling, H., White, D., & Rangarajan, F. V. N. 2001, MNRAS, submitted
 Elmouttie, M., Haynes, R. F., Jones, K. L., Sadler, E. M., & Ehle, M. 1998, MNRAS, 297, 1202
 Evans, D. W. 1989, A&AS, 78, 249
 Fabbiano, G. 1989, ARA&A, 27, 87
 Fabbiano, G., Zezas, A., & Murray, S. 2001, ApJ, in press
 Fox, D. W., et al. 2000, MNRAS, 319, 1154
 Freeman, K. C., Karlsson, B., Lynga, G., Burrell, J. F., van Woerden, H., Goss, W. M., & Mebold, U. 1977, A&A, 55, 445
 Freeman, P. E., Kashyap, V., Rosner, R., & Lamb, D. Q. 2001, ApJ, submitted

- Garcia, M. R., Murray, S. S., Primini, F. A., Forman, W. R., McClintock, J. E., & Jones, C. 2000, *ApJ*, 537, L23
- Gehrels, N. 1986, *ApJ*, 303, 336
- Greiner, J., Morgan, E. H., & Remillard, R. A. 1996, *ApJ*, 473, L107
- Griffiths, R. E., Ptak, A., Feigelson, E. D., Garmire, G., Townsley, L., Brandt, W. N., Sambruna, R., & Bregman, J. N. 2000, *Science*, 290, 1325
- Guainazzi, M., et al. 1999, *MNRAS*, 310, 10
- Helfand, D. J. 1984, *PASP*, 96, 913
- Høg, E., et al. 2000, *A&A*, 355, L27
- Houck, J. C., Bregman, J. N., Chevalier, R. A., & Tomisaka, K. 1998, *ApJ*, 493, 431
- Immler, S., Pietsch, W., & Aschenbach, B. 1998, *A&A*, 331, 601
- Immler, S., Pietsch, W., & Aschenbach, B. 1998, *A&A*, 336, L1
- Kohmura, Y., et al. 1994, *PASJ*, 46, L157
- Kraft, R. P., Burrows, D. N., & Nousek, J. A. 1991, *ApJ*, 374, 344
- Lasker, B. M., Sturch, vC. R., McLean, B. J., Russell, J. L., Jenkner, H., & Shara, M. M. 1990, *AJ*, 99, 2019
- Lira, P., Lawrence, A., & Johnson, R. A. 2000, *MNRAS*, 319, 17
- Lockman, F. J. & Savage, B. D. 1995, *ApJS*, 97, 1
- Lyons, L. 1991, *Data Analysis for Physical Science Students*. (Cambridge: Cambridge University Press)
- Maccacaro, T., Gioia, I. M., Wolter, A., Zamorani, G., & Stocke, J. T. 1988, *ApJ*, 326, 680
- Maiolino, R., Alonso-Herrero, A., Anders, S., Quillen, A., Rieke, M. J., Rieke, G. H., & Tacconi-Garman, L. E. 2000, *ApJ*, 531, 219
- Makishima, K., et al. 2000, *ApJ*, 535, 632
- Marconi, A., Moorwood, A. F. M., Origlia, L., & Oliva, E. 1994, *The ESO Messenger*, 78, 20
- Matt, G., et al. 1996, *MNRAS*, 281, L69
- Mitsuda, K., et al. 1984, *PASJ*, 36, 741
- Morrison, R., & McCammon, D. 1983, *ApJ*, 270, 119
- Motch, C., et al. 1998, *A&AS*, 132, 341
- Mukai, K. 2000, *PIMMS Version 3.0 Users' Guide*. NASA/GSFC, Greenbelt
- Oliva, E., Marconi, A., Cimatti, A., & Alighieri, S. D. 1998, *A&A*, 329, L21
- Oliva, E., Salvati, M., Moorwood, A. F. M., & Marconi, A. 1994, *A&A*, 288, 457
- Osterbrock, D. E. 1989, *Astrophysics of Gaseous Nebulae and Active Galactic Nuclei* (Mill Valley: University Science)
- Paczyński, B. 1971, *ARA&A*, 9, 183
- Pooley, D., et al. 2001, *astro-ph/0103196*
- Pringle, J. E., & Wade, R. A. 1985, *Interacting Binary Stars* (Cambridge: Cambridge University Press)
- Raymond, J. C., & Smith, B. W. 1977, *ApJS*, 35, 419
- Roberts, T. P., & Warwick, R. S. 2000, *MNRAS*, 315, 98
- Ruiz, M., Alexander, D. M., Young, S., Hough, J., Lumsden, S. L., & Heisler, C. A. 2000, *MNRAS*, 316, 49
- Sambruna, R. M., Brandt, W. N., Chartas, G., Netzer, H., Kaspi, S., Garmire, G. P., Nousek, J. A., & Weaver, K. A. 2001, *ApJ*, 546, L9
- Sambruna, R. M., Netzer, H., Kaspi, S., Brandt, W. N., Chartas, G., Garmire, G. P., Nousek, J. A., & Weaver, K. A. 2001, *ApJ*, 546, L13
- Sarazin, C. L., Irwin, J. A., & Bregman, J. N. 2000, *ApJ*, 544, L101
- Schlegel, E. M. 1995, *Reports of Progress in Physics*, 58, 1375
- Schlegel, D. J., Finkbeiner, D. P., & Davis, M. 1998, *ApJ*, 500, 525
- Shirey, R., et al. 2001, *A&A*, 365, L195
- Stetson, P. B. 1987, *PASP*, 99, 191
- Stetson, P. B. 1996, *PASP*, 108, 851
- Sugizaki, M., Matsuzaki, K., Kaneda, H., Yamauchi, S., & Mitsuda, K. 1999, *Astronomische Nachrichten*, 320, 383
- Taniguchi, Y., Shioya, Y., Tsuru, T. G., & Ikeuchi, S. 2000, *PASJ*, 52, 533
- Tennant, A. F., Wu, K., Ghosh, K. K., Kolodziejczak, J. J., & Swartz, D. A. 2001, *ApJ*, submitted
- Verbunt, F., & van den Heuvel, E. P. J. 1995, in *X-ray Binaries*, ed. W. H. Lewin, J. Van Paradijs, & E. P. J. van den Heuvel (Cambridge: Cambridge University Press), p. 457
- Warner, B. 1995, *Cataclysmic Variable Stars* (Cambridge: Cambridge University Press)
- Watarai, K., Mizuno, T., & Mineshige, S. 2001, *ApJ*, in press, (*astro-ph/0011434*)
- White, N. E., Nagase, F., & Parmar, A. N. 1995, in *X-ray Binaries*, ed. W. H. Lewin, J. Van Paradijs, & E. P. J. van den Heuvel (Cambridge: Cambridge University Press), p. 1
- Wilson, A. S., Shopbell, P. L., Simpson, C., Storchi-Bergmann, T., Barbosa, F. K. B., & Ward, M. J. 2000, *AJ*, 120, 1325
- Yokogawa, J., Imanishi, K., Tsujimoto, M., Nishiuchi, M., Koyama, K., Nagase, F., & Corbet, R. H. D. 2000, *ApJS*, 128, 491